THREE DIMENSIONAL DYNAMICS IN THE WAKE OF AN AHMED BODY

Bérangère Podvin, Stéphanie Pellerin, Y. Fraigneau, Olivier Cadot

55th 3AF International Conference on Applied Aerodynamics
23 – 25 March 2020, Poitiers - France

FP84-AERO2020-pellerin

THREE DIMENSIONAL DYNAMICS IN THE WAKE OF AN AHMED BODY

Bérengère Podvin[(1)], Stéphanie Pellerin[(2)], Yann Fraigneau[(1)] and Olivier Cadot[(3)]
[(1)] LIMSI, CNRS, Université Paris-Saclay, Bât 507, Campus Universitaire F-91405 Orsay, France, Email: berengere.podvin@limsi.fr
[(2)] LIMSI, CNRS, Univ. Paris-Sud, Université Paris-Saclay, Bât 507, Campus Universitaire F-91405 Orsay, France, Email: stephanie.pellerin@limsi.fr
[(3)] University of Liverpool, School of Engineering, Brodie Tower (Building No. 233), Liverpool L69 3BX, UK, Email: Olivier.Cadot@liverpool.ac.uk

ABSTRACT

A flow around a squareback Ahmed body is simulated with a DNS using the 3D parallel in-house code *SUNFLUIDH*. A penalization method is applied for the body. The DNS recovers the deviation of the wake observed experimentally [1]. POD is first applied in a plane section in the near wake at mid-height of the body and allows a comparison with experiments. The spatial modes and the histograms of the amplitudes are similar and two main frequencies are extracted, which are related to vortex shedding and wake pumping phenomena. A 3-D POD is then applied to the full velocity field and leads to a better understanding of the deviation phenomenon, linked to the second mode. Moreover, a POD-based low dimensional model captures the main frequencies of the modes in the simulation and correctly estimates the energetic content. This shows the predictive ability of the model.

1. INTRODUCTION

In flows over bluff-bodies, deviation of the wake associated with bistability was observed in experiments [1] and more recently in LES [2]. In past numerical studies, we have simulated the flow over a squareback Ahmed body with a LES approach and analyzed the influence of the ground clearance and the Reynolds number on the dynamics of the wake [3,4,5].

This study is based on a DNS in-house code [6] and focuses on different topics. Using POD, we first complete the comparison with our reference experiment, in the near wake, and try to identify characteristic frequencies and associated processes. Therefore, a 3D POD is applied to the full flow to give a precise analysis of frequencies. Then, a POD low dimensional model is developed and applied to the DNS data to lead to a classification of phenomena.

In the next part the configuration of the flow studied is presented, then the DNS code used, and the characteristics of the simulation. The section 3 concerns the flow resolved using DNS and focuses on the deviation of the wake. The POD approach is detailed in section 4. The DNS results are compared with experimental PIV data, through a POD treatment, in section 5. POD is then applied (section 6) to the full field to extract the dynamics of the wake. The reduced POD model is developed and applied in section 7.

2. CONFIGURATION

2.1 Geometry

A flow around a squareback Ahmed body is simulated with DNS. The chosen profile corresponds to an experimental model of Evrard *et al.* [7]. The dimensions of the body are $L=3.78H$ (length) and $W=1.18H$ (width), where H is the height of the vehicle and the characteristic length of the problem.

The simulation considers a ground clearance of $30\%H$. The Reynolds number, equal to 10^4, is based on H, the upstream velocity U_∞ and the viscosity of the fluid ν_{air}. The time unit corresponds to H/U_∞ and all the times will be expressed in these units.

Note that the reference experiment corresponds to higher Reynolds number equal to 4×10^5. However, previous observations suggest that the dynamics of the wake are not very sensitive to the Reynolds number in this range of parameters.

2.2 DNS code

The simulation is performed using the 3D parallel in-house code *SUNFLUIDH*, based on a second-order finite volume approach, whose details are given in [6].

A second-order backward Euler scheme is used for the temporal discretization. Diffusion terms are treated implicitly and convective terms are solved with an Adams-Bashforth scheme. The Poisson equation for the computation of pressure field is solved iteratively.

The body is modelled by a pseudo-penalization method. No-slip velocity boundary conditions on the Ahmed body and on the ground are imposed on the physical boundaries.

2.3 Simulation

The propagation direction is *(x)*, the spanwise direction *(y)* and the vertical direction *(z)*. The computational grid is *nx(512)×ny(256)×nz(256)* points, and corresponds to 33.5 million points. In order to correctly describe the turbulent boundary layers, the Cartesian grid is refined close to surfaces, with a value of $Y^+ = 1$ imposed for the first local cell close to the walls. Periodic boundary conditions are applied in the spanwise direction, on a regular grid.

The computational domain for the *(x×y×z)* directions is *[−1,10]H×[−2,2]H×[−1.3,1.2]H*. The Ahmed body is centered in the spanwise *(z)* direction and placed at the chosen ground clearance of *30%H* on the vertical direction *(y)*. So, the mid-plane of the body is at *y=0*. The origin of the domain is located on the roof (*z=0*) and nose (*x=0*) of the body. Results are mainly presented in the mid-height plane of the body at *z=0.5H*, which also corresponds to the PIV plane in the experiment.

The flow is initially at rest and develops over the long time of about 100 time units to reach statistical convergence.

3. DEVIATION OF THE WAKE

The unsteady flow is represented in terms of vertical vorticity ω_z in the mid-height plane of the body (Fig. 1). The simulation captures the different characteristics of this turbulent flow. A first upstream separation occurs along the body, with ejection of dipoles vortices. At the end of the body, mixing layers develop and surround a recirculation zone. The 3D structures associated with a shedding process are complex.

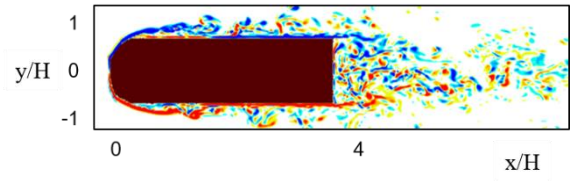

Figure 1. Vertical vorticity ω_z, performed by DNS: zoom of the unsteady flow over a squareback Ahmed body, in its mid-height *(xy)* plane *(z/H=-0.5)*.

In this configuration, experiments have shown that, for a sufficiently large value of the ground clearance, the wake is deviated towards one or the other side of the body, thereby breaking the symmetry with respect to the mid-span plane of the body. The deviations remain quasi-steady over large periods of time, but random switches from one side to the other are observed, indicating the presence of multistability. As a result, the statistical symmetry of the flow is restored over very long time scales. The duration of the switches is small compared to the time over which the deviation remains along one side. In this study, the switches take place in the spanwise direction, due to the value of the aspect ratio *W/H>1* [1], and can then be observed in the horizontal mid-height plane (*z/H=-0.5*).

As was observed with our LES code [3,4,5], the asymmetry in the near wake at mid-height of the body observed in the experiment is recovered in the DNS as can be seen in Fig. 2.left, which shows the time-averaged velocity field. We note that wake flow is consistently asymmetric in the vertical plane, due to the presence of the ground at *30%H* bellow the body, as can be seen in Fig. 2.right, which shows a side-view in the mid-span plane of the mean flow.

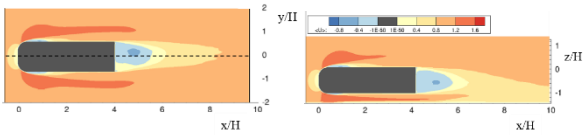

Figure 2. Longitudinal time-averaged flow $\langle v_x \rangle$ simulated by DNS: (left) mid-height plane of the body (*z/H=-0.5*); (right) mid-span plane (*y/H=0*); the ground is at *z/H=-1.3*.

The spanwise asymmetry detected in the time-averaged flow in the simulation is likely to be a consequence of the short duration of the simulation, as the simulation is unable to reproduce switches which are characterized by a very low frequency. However the high time resolution of the simulation makes it possible to characterize events occurring on small time scales. In contrast, the experiment spans long time scales, with a time resolution which is much lower than the simulation. As a consequence, it is not possible to extract from the available experimental data the characteristic time scales of vortex shedding or wake pumping. The experimental and the numerical datasets therefore constitute two almost disjoint sets of frequencies associated with different physics, which makes comparison potentially difficult. In the next section we describe how our analysis will be specifically designed to deal with this discrepancy.

4. ANALYSIS TOOLS

4.1 POD

Proper Orthogonal Decomposition (POD) is applied to different subdomains of the flow in order to extract the main structures of the flow and provide some understanding of its dynamics. Furthermore the POD functions provide a basis onto which the Navier-Stokes equations can be projected, thus giving way to a low-dimensional model for the flow dynamics. The reader is referred to [8] for an in-depth discussion of POD. The basic idea of POD is to expresss the velocity field as a linear combination of spatial functions (which we call POD modes), the amplitude of which varies in time. We therefore have

$$\underline{u}(\underline{x},t) = \sum_{n>1} a^n(t)\, \underline{\varphi}^n(\underline{x}) \qquad (1)$$

These functions φ are actually eigenfunctions of the spatial autocorrelation tensor C:

$$\int C\ (\underline{x},\underline{x}') \cdot \underline{\varphi}(\underline{x}')d\underline{x}' = \lambda \cdot \underline{\varphi}(\underline{x}) \qquad (2)$$

These functions can be ordered according to the value of λ, which represents the magnitude of the contribution of these functions to the aucorrelation tensor $C(\underline{x},\underline{x}') = \langle \underline{u}(\underline{x},t)\, \underline{u}(\underline{x}',t) \rangle$ where <> is a time average.

The amplitudes of the POD eigenfunctions can be recovered from the full velocity field using

$$a^n(t) = \int \underline{u}(\underline{x},t) \cdot \underline{\varphi}^n(\underline{x})\, d\underline{x} \qquad (3)$$

The method of snapshots (see [9]) is used for POD implementation. The autocorrelation tensor is built from the N available flow realizations, also called set of snapshots

$$C(\underline{x},\underline{x}') = \frac{1}{N} \sum_{i=1}^{N} \underline{u}(\underline{x},t_i)\, \underline{u}(\underline{x}',t_i) \qquad (4)$$

4.2 Symmetry

A central question of this paper is to make a relevant comparison between the simulation and the experiment. As noted above, the issue is that the simulation time is short, so that no switches are observed in the wake, and the full space of possible configurations is not correctly explored. Due to bistability, this space is characterized by symmetry: the image of any flow realization by the reflection symmetry S with respect to the mid-span plane of the body is also a possible flow realization. The idea that we will therefore implement here is to work in an augmented realization space where the images of all flow realizations through S are used to construct the set of snapshots. This augmentation will be applied to the numerical simulation as well as the experiment, this making it possible to recover deviations on both sides in the numerical simulation. However an important point is that this procedure does not make it possible to capture the switches observed in the experiments. The corresponding portion of configuration space is therefore missing from the numerical data, even with the augmentation. We therefore do not expect to be able to describe the details of the switching process and in particular to identify a specific instability mechanism in the simulation. However, due to the short duration of the switches, we do not expect this missing data in the simulation to affect the description of the quasi-steady deviation states.

We now examine the consequences of this symmetry for the eigenvalue problem. The main result is that due to the existence of the symmetry, the eigenfunctions of the problem are necessarily purely symmetric or antisymmetric with respect to S. Let us suppose that an eigenfunction φ is solution of the problem

$$C(\underline{x},\underline{x}') \cdot \underline{\varphi}(\underline{x}')d\underline{x}' = \lambda\, \underline{\varphi}(\underline{x}) \qquad (5)$$

It is easy to see that its image S φ satisfies the same equation.

$$\int C(S\varphi) = \lambda\, (S\varphi) \qquad (6)$$

Since any function can be split into its symmetric and antisymmetric part,

$$f = f_s + f_a \qquad (7)$$

one can also see that both the symmetric part and the antisymmetric parts of the eigenfunctions are also eigenfunctions associated with the same eigenvalues, as well as any linear combination of the symmetric and antisymmetric parts of the eigenfunction. This gives rise to an unlimited denegeracy of the eigenproblem, which is not possible, unless the eigenfunctions are purely symmetric or antisymmetric.

5. COMPARISON WITH A REFERENCE EXPERIMENT

The experiment provides PIV data on a plane horizontal section in the near wake at mid-height of the body. We first apply POD in the equivalent numerical zone to compare the spatial modes and the temporal evolutions with the experiment. The time step between two snapshots is very small for the numerical data with 0.5 time units, and much larger for experimental data with 25 time units.

A very good agreement is observed, even if the Reynolds number is lower in the DNS, for the spatial modes (Fig. 3) and the histograms of the amplitudes (see [10]). Using the symmetrical process presented before, the first spatial mode corresponds to the time-averaged flow and it is then symmetric. The second mode is associated with the deviation phenomenon. This comparison permits to extract main frequencies, which are all low frequencies. Two main frequencies are identified, $f_{VK} = 0.2$, which is associated to the vortex shedding (antisymmetric modes 4, 5 and 6), and

f_{WP} = 0.08, related to the wake pumping phenomena (symmetric modes 3 and 7).

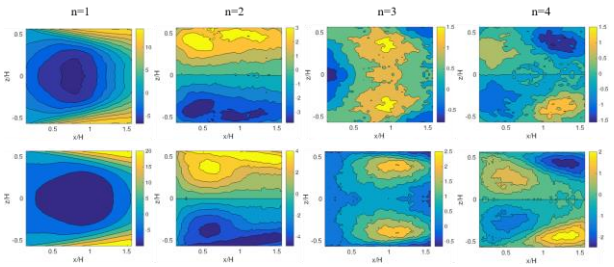

Figure 3. 2D-POD in the near wake, on a mid-height plane of the body (z/H=-0.5) and a chosen section; spatial modes 1 to 4, (top) DNS and (bottom) experiment

6. POD OF THE FULL FIELD

A 3D-POD approach is then considered using the full 3D velocity field. Spatial modes are again symmetric or antisymmetric. For this 3D profile, concerning the vortex shedding, the two frequencies associated with the dimensions of the body H and W are present (Fig. 4).

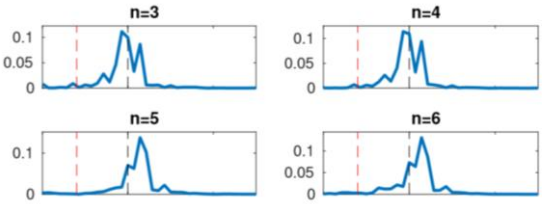

Figure 4. Power spectral density of the 3D-POD 3 to 6 modes amplitudes in the simulation

The main objective is a better understanding of the switch phenomenon, linked to the second mode. This analysis shows that the amplitude of the deviation mode on the full domain is well estimated from 2-D near wake data, and that it is the main energetic mode.

In addition, there is a negative correlation between the magnitude of the deviation (amplitude of mode 2) and the intensity of the shedding modes in the horizontal direction (defined as the square root of the energy of modes 3 and 4) as can be seen from figure 5. This is interesting, as peaks of shedding intensity correspond to minima in wake deviation in the simulation, which is interesting, as switches observed experimentally have been found to be associated with local intensification of the shedding process. Furthermore, one can show that the deviation intensity is positively correlated with the evolution of the drag [10].

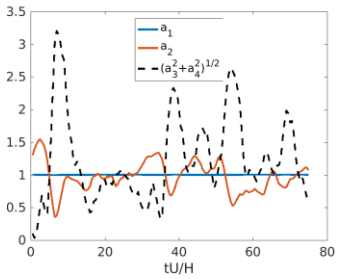

Figure 5. Amplitudes Time evolution of the amplitudes of the POD modes – the deviation mode (a_2) and the intensity of the modes associated with horizontal vortex shedding $(a_3^2+a_4^2)^{1/2}$

7. POD LOW DIMENSIONAL MODEL

Moreover, it is possible to project the Navier-Stokes equations onto the basis of eigenfunctions to recover a set of ode's for the problem. The model derivation procedure is described in [10]. The effect of the unresolved modes is taken into account to close the model. Integration of the dynamical system shows that the main frequencies of the simulation are correctly captured by the model and that the energetic content is satisfactorily reproduced. Then, a POD-based low dimensional model captures the main frequencies of the modes in the simulation and correctly estimates the energetic content (Fig. 6). This shows the predictive ability of the model.

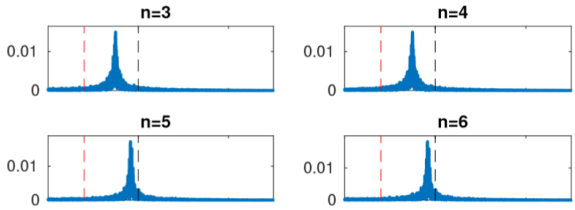

Figure 6. Power spectral density of the 3D-POD 3 to 6 modes amplitudes in the model

Comparison of phase portraits (Fig. 7) shows this good agreement.

The amplitude of the second mode, the deviation mode, can then be reconstructed and displays along a large number of switches, in agreement with experimental observation [10].

A striking feature is that the model is able to produce switches in the deviation mode on a time scale that is in good agreement with the experiments, although the time scale of the DNS is not sufficient for switches to be observed. This shows the complemental role of experiments and simulations to obtain understanding of the dynamics of the flow and particularity of its near wake.

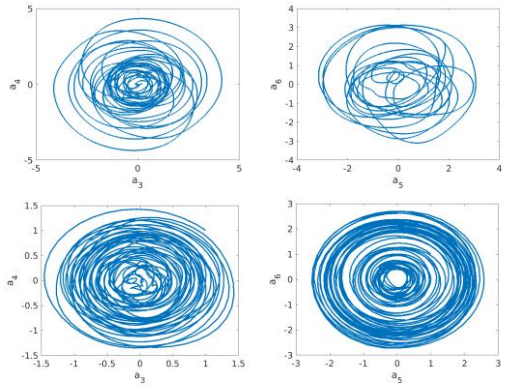

Figure 7. Phase portraits of 3D-POD mode amplitudes: (left) a_3-a_4 plane, (right) a_5-a_6 plane; (top) simulation, (bottom) reduced model

8. CONCLUSION

Numerical simulation of the flow around an Ahmed body was used to carry out a comparison with the experiment and to investigate the dynamics of the wake flow. The comparison relies on Proper Orthogonal Decomposition, a statistical tool to extract coherent motion in the flow. Due to the short duration of the simulation, it was not possible to explore both types of quasi-steady states observed in the experiment. However a suitable framework for comparison could be obtained by augmenting the original dataset through application of symmetry to individual realizations, thus fully enforcing statistical symmetry in both numerical and experimental configurations. 2D application of the procedure to plane measurements showed a good agreement between the experiment and the simulation despite a discrepancy in Reynolds number and differences in the ground clearance. Full 3-D spatio-temporal analysis made it possible to connect the well-known wake deviation mode, vortex shedding modes, and wake pumping motion with POD structures. A low-dimensional model was derived by projection of the Navier-Stokes equations onto the basis of POD eigenfunctions. The dynamics predicted by the model were found to reproduce relatively well those observed in the simulation.

9. REFERENCES

1. Grandemange, M., Gohlke, M. & Cadot, O. (2013). Turbulent wake past a three-dimensional blunt body Part 1 – global modes and bi-stability. *J. Fluid Mech.*, 722, 1-26.

2. Dalla Longa, L., Evstafyeva, O. & Morgans, A.S. (2019). Simulations of the bi-modal wake past three-dimensional blunt bluff bodies. *J. Fluid Mech.*, 866, 791809.

3. Pellerin, S. & Podvin, B. (2015). A study of the ground influence on the wake of an Ahmed body profile. *50th 3AF International Conference on Applied Aerodynamics*, Toulouse, France, 30-31 March - 1 April.

4. Pellerin, S., Podvin, B. & Cadot, O. (2016). Numerical study of the RSB wakes of an Ahmed body. *Aerovehicles 2*, Chalmers University, Göteborg, Sweden, June 21-23.

5. Pellerin, S., Podvin, B. (2018). Analysis and control of the symmetry breaking wakes behind an Ahmed body by Large Eddy Simulation. *Aerovehicles 3*, Milano, Italy, June 13-15.

6. Podvin, B. & Fraigneau, Y. (2017). A few thoughts on proper orthogonal decomposition in turbulence. *Physics of Fluids*, 29:020709.

7. Evrard, A., Cadot, O., Herbert, V., Ricot, D., Vigneron, R., and Delery, J. (2016). Fluid force and symmetry breaking modes of a 3d bluff body with a base cavity. *J. Fluids Struc.*, 61, 99–114.

8. Lumley, J.L. (1967). The structure of inhomogeneous turbulent flows. In A.M Iaglom and V.I Tatarski, editors, Nauka, Moscow. *Atmospheric Turbulence and Radio Wave Propagation*, 221–227.

9. Sirovich, L. (1987). Turbulence and the dynamics of coherent structures part i: Coherent structures. *Quart. Appl. Math.*, 45(3), 561–571.

10. Podvin, B., Pellerin, S., Fraigneau, Y., Evrard, A. & Cadot, O. Proper Orthogonal Decomposition Analysis and Modelling of the wake deviation behind a squareback Ahmed body. arXiv 1909.13129.